Correlation between Local and Global Inhomogeneities of Chemical Gels

ARTICLE *in* MACROMOLECULES · DECEMBER 2013

Impact Factor: 5.8 · DOI: 10.1021/ma400486h

Macromolecules

Article

pubs.acs.org/Macromolecules

Correlation between Local and Global Inhomogeneities of Chemical Gels

Makoto Asai,*[†,§] Takuya Katashima,[‡] Ung-il Chung,[‡] Takamasa Sakai,[‡] and Mitsuhiro Shibayama[†]

[†]Institute for Solid State Physics, The University of Tokyo, 5-1-5, Kashiwanoha, Kashiwa, Chiba 277-8581, Japan

[‡]Department of Bioengineering, School of Engineering, The University of Tokyo, 7-3-1, Hongo, Bunkyo-ku, Tokyo 113-8656, Japan

ABSTRACT: It is well-known that mechanical properties of gels are strongly related to inhomogeneities of gels such as spatial and connectivity inhomogeneities (defects and variation of cycles). Here, a cycle is defined as the type of polygonal shape formed by several prepolymers. However, these inhomogeneities, especially connectivity inhomogeneities, have hardly been quantified due to the difficulty in directly observing them. To directly observe and analyze gel structures, we used a molecular dynamics simulation to reproduce gelation process and quantified defects and cycles of the obtained gels. Furthermore, we investigated the relation between defects or cycles and spatial inhomogeneities. Our investigation indicated that defects caused spatial inhomogeneities in dilute and semidilute systems. On the other hand, in concentrated systems, self-biting links, in which a cross-link connects with itself, caused spatial inhomogeneities. This could be observed in the swollen state, which is revealed in the difference in degree of swelling of cycles during the swelling process.

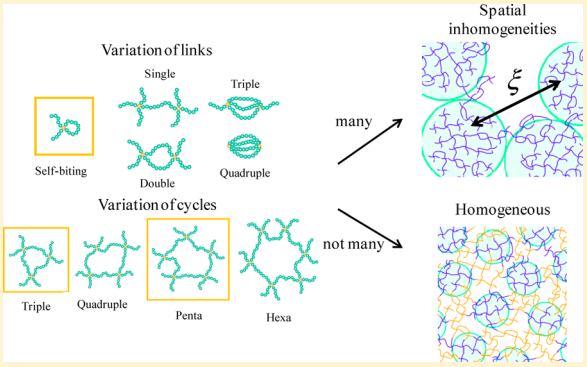

INTRODUCTION

Chemical gels are industrially promising materials which can be used in applications such as water absorbent, water container, and shock absorber. Lately, chemical gels have been investigated for applications in bioengineering, for example as artificial scaffolds for tissue regeneration and drug reservoirs for drug delivery systems. Their significance is further increasing.[1−4]

However, there are numerous unsolved phenomena concerning gels. A representative example is the relationship between a gel's structure and its mechanical properties. Typical gels are mechanically weak. This brittleness of gels, which limits their range of application, has been attributed to the various types of inhomogeneities within gels.[5−10] Shibayama, one of the authors of this paper, suggested that inhomogeneities in the static structure of gels could be classified in the following three categories: connectivity, topological, and spatial.[11] Connectivity inhomogeneities include variations in links between cross-links and variations in cycles formed by several prepolymers. Topological inhomogeneities are entanglements of polymer chains. Spatial inhomogeneities are density variations in space. In terms of their configurationality, in this paper we categorize connectivity and topological inhomogeneities as local and spatial inhomogeneities as global.

There have been many reports on the analysis of spatial inhomogeneities. These analyses mainly use small-angle neutron scattering (SANS)[12−16] and static light scattering,[17−19] which have quantified spatial inhomogeneities as density fluctuations within gels.

It has been supposed that global inhomogeneities might be caused by local inhomogeneities. Therefore, over the past several years, many researchers have developed a "model network" that is designed to form an ideal polymer network in the absence of any kind of local inhomogeneities. These studies are largely categorized into two approaches. One is to form gels using an asymmetrical combination of multifunctional cross-linkers and linear polymers,[20−23] which we call end-cross-linking gels (EC gels). Another approach is to form gels using a symmetrical combination of multifunctional prepolymers, which we call cross-link-coupling gels (CC gels). Note that the same network structure would be formed by both approaches if the gelation process progressed ideally. The difference between the approaches is in the way that they divide the prepolymer unit (see Figure 1).

However, previous studies have indicated that the model network obtained in the EC approach contains some kinds of inhomogeneities.[24−26] On the other hand, Sakai et al. have developed tetrabranched poly(ethylene glycol) (Tetra-PEG) using an A−B type CC approach[27] and have reported practically no spatial inhomogeneity.[28] Although both approaches were designed to create the same ideal network, they created different gel structures. This issue has long been an unsolved challenge in physics of gels. It has been presumed that local inhomogeneities within the gel are the main cause, and thus many studies on local inhomogeneities have been conducted. Previous theoretical studies,[29−31] experiments,[32−35] and simulations[36−45] have shown that polymer gels contain 2−20% local inhomogeneities and that the amount of inhomogeneities seems to strongly depend on the structure of the prepolymer. Of all types of inhomogeneities, an

Received: March 6, 2013
Revised: November 29, 2013

   dx.doi.org/10.1021/ma400486h | *Macromolecules* XXXX, XXX, XXX−XXX

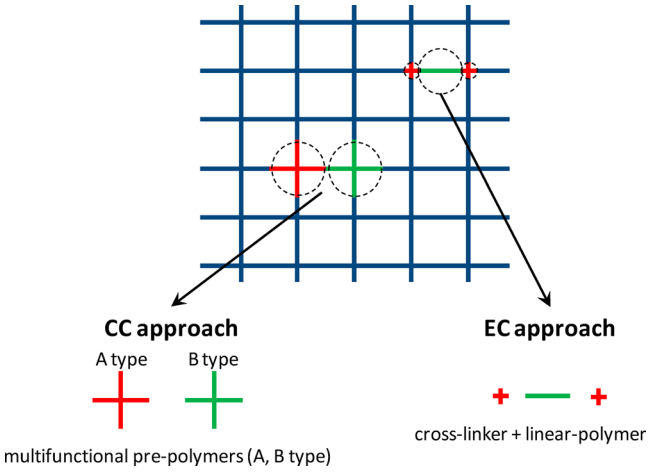

Figure 1. Schematic of A−B type CC and EC approaches. This image is two-dimensional, though the simulation is three-dimensional.

elastically inactive structure called the "dangling loop" has been the center of focus. This structure not only degrades elasticity but may also prevents the formation of a uniform three-dimensional network. Hence, it has been thought to be the cause of spatial inhomogeneities. Recently, Schwenke et al. have used the bond-fluctuation model[46] to simulate and analyze the connectivity of homopolymer star networks (in which all reactive groups are of the same type A) and copolymer star networks (in which there is a stoichiometric mixture of A and B type stars that exclusively forms A−B bonds). Both star networks are composed of four-arm star polymers with equal arm length. The copolymer star networks, also called A−B networks, model the Tetra-PEG gel. The authors found that dangling loops dominated in A-type networks while A−B networks had a more uniform network structure. However, from the analysis of the pair-correlation function and the scattering function, they concluded that A−B networks did not have a diamond lattice structure but rather an amorphous packing of A- and B-type stars. Moreover, Lange et al. used NMR measurements to quantify bond types between neighboring stars within Tetra-PEG gel. Since neighboring stars bonded by one arm are "ideal", then neighboring stars bonded by more than one arm were categorized as "defects". Although most defects are elastically active, they are also presumed to degrade elasticity from the perspective of stress distribution. From the NMR results, it was found that the Tetra-PEG gels contained up to 50% defects. The defect fraction decreased as concentration increased, so that the defect fraction could be decreased to as much as 20%. However, this defect fraction is comparable to that of other types of gels. Therefore, it remains a mystery why, despite the large amount of defects, Tetra-PEG gels are mechanically stronger than conventional gels and do not have spatial inhomogeneity.

In our study, we tackled this problem by redefining what local inhomogeneities are considered defects that could affect spatial inhomogeneities, and we compared A−B network gels with conventional gels. We performed coarse-grained molecular dynamics simulations to reproduce gelation process in EC gels and A−B type CC gels (hereafter referred to simply as "CC gels"). We quantified spatial inhomogeneities and connectivity inhomogeneities (links and cycles) and investigated the correlation between them.

MODELS AND METHODS

Kremer−Grest model. We used the Kremer−Grest model (KG model),[47] a coarse-grained model of polymer chains. Previous studies have indicated that the KG model is a highly versatile model that can reproduce the various scaling relations of polymer chains from a dilute system to a melt.[47] In this model, a polymer chain is coarse-grained as blobs with size that hold Gaussian statistics, and these blobs are connected by the finitely extensible nonlinear elastic potential (FENE), and the excluded volume interactions between all blobs are described by a shifted Lennard-Jones (LJ) 12−6 potential:

$$\text{(LJ)} \quad U^{\text{LJ}} = 4\varepsilon\left[\left(\frac{r}{r_{ij}}\right)^{12} - \left(\frac{r}{r_{ij}}\right)^{6}\right] + c \tag{1}$$

$$\text{(FENE)} \quad U^{\text{F}} = \frac{1}{2}kR_0 \ln\left[1 - \left(\frac{r}{R_0}\right)^2\right] \tag{2}$$

where r_{ij} is the distance between ith and jth blobs in units of σ, and ε is the well depth of the potential. The LJ potential has a minimum at $r = 2^{1/6}\sigma$ ($\equiv r_{\text{min}}$). The cutoff distance r_{cutoff} was set to $2r_{\text{min}}$ to reduce computational time, with constant $c = 0.007\,75$ chosen such that U^{LJ} ($r = r_{\text{cutoff}}$) = 0. Here, σ, ε, and τ are the dimensionless physical constants for distance, energy, and time, respectively. In the present work, we have chosen $\sigma = 1$. The values of other parameters were chosen to be the same as standard parameters used in the Kremer−Grest force field,[47] including the maximum bond length $R_0 = 1.5\sigma$ and the spring coefficient $k = 30\varepsilon\sigma^{-2}$, which ensures that chains do not intersect.

Structure of Prepolymer. The structures of prepolymers used for EC and CC gels are shown in Figure 2. For an EC gel, a cross-linker is represented as a single terminal blob ($N_{\text{b}} = 1$). Each linear prepolymer consists of 20 blobs ($N_{\text{b}} = 20$). During the simulation, a bond may form between a cross-linker and the terminal blob of a linear prepolymer ("end-cross-linking"). Each cross-linker can bond with up to four terminal blobs of linear polymers. Therefore, the ratio of cross-linkers and linear polymers was set to 1:2, where the number of cross-linkers is $N_{\text{c}} = 1000$ and the number of linear polymers is $N_{\text{p}} = 2000$. For an A−B type CC gel, we used tetrabranched (TB) star polymers with four chains consisting of 10 blobs each ($N_{\text{b}} = 10$). Note that a terminal blob of a TB star polymer can only bond with terminal blobs of different type. The ratio of type A and B was set to 1:1, with $N_{\text{p}} = 1000$ TB star polymers of each type. In our system, when the distance between terminal blobs is $\leq r_{\text{min}}$, a new bond is formed with probability 1. If EC and CC gels were obtained ideally, their cross-links would be arranged as a diamond lattice.

Motion Equations of Blobs. The motion of blobs was driven by Langevin dynamics according to eq 3, with a time step of 0.005τ, temperature $T = 20.0\varepsilon/k_{\text{B}}$, and friction $\Gamma = 40.0$, where T and Γ were chosen to both prevent both chain intersection and reduce computational time.

$$\frac{\mathrm{d}\mathbf{r}^2}{\mathrm{d}t} = -\frac{\mathrm{d}U}{\mathrm{d}\mathbf{r}} - \Gamma\frac{\mathrm{d}\mathbf{r}}{\mathrm{d}t} + \mathbf{R}(t) \tag{3}$$

Equation 3 is the governing motion equation for our simulation, where $\mathbf{r}$ is the position vector of a blob. The first term on the right-hand side of eq 3 is the force contribution from the potentials, the second is a viscous term, and the third is a random force $\mathbf{R}(t)$, satisfying the following equations:

$$\langle \mathbf{R}(t) \rangle = 0 \tag{4}$$

$$\langle \mathbf{R}_i(t)\mathbf{R}_j(t') \rangle = 6\Gamma k_{\text{B}}T\sigma_{ij}\sigma(t - t') \tag{5}$$

dx.doi.org/10.1021/ma400486h | Macromolecules XXXX, XXX, XXX−XXX

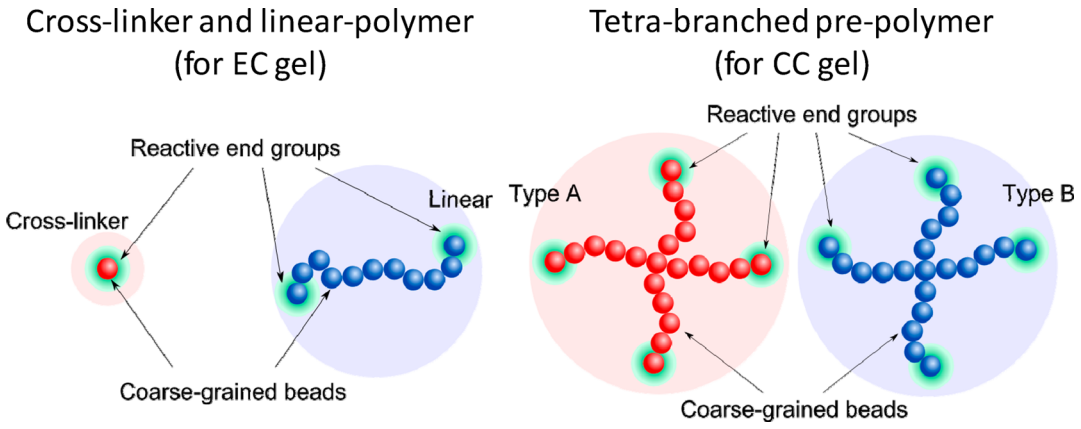

Figure 2. Coarse-grained model of prepolymers for EC (left) and CC (right) gels. Spheres represent blobs. Red and blue prepolymers can only connect with one another. The blobs with a green halo represent reactive ends (terminal blobs). Note that the numbers of blobs within the chains in the illustration is different from those actually used in this work.

where the angle brackets represent a statistical average. Equation 5 shows the correlation of the random force between the ith blob at time t and the jth blob at time t'. In this study, the solvent is considered implicitly via the viscous term and the random force, representing thermal noise. We define p as the fraction of terminal blobs that have reacted. To stabilize the prepolymer structure, 3×10^7 MD steps were executed initially without the gelation reaction. Then geleation was switched on, and calculations were executed until $p = 0.95$ (the final state). The number of MD steps required to reach the final state differed for each system; the longest was 200 million MD steps. We simulated five times for each set of conditions. The gel point (percolation point) is defined as the point when the extent of the largest cluster formed during gelation process exceeds the simulation cell in the x, y, and z directions, and the p at this point is defined as p_c. The concentration of the gel is defined as the volume fraction $\phi_0 = V_p/V$, where V is the volume of simulation box and V_p is the occupied volume of prepolymers.

RESULTS AND DISCUSSION

Overlap Concentration. First, we determine the overlap concentration ϕ^* in our model, which is defined as the concentration in which neighboring prepolymers start to interact with each other. The concentration region around ϕ^* is called the "semidilute regime." When one compares prepolymers with different structures, one should universally discuss the gelation process by using a normalized concentration defined as $\Phi \equiv \phi_0/\phi^*$, instead of ϕ_0. We investigated the ϕ_0-dependence of the radius of gyration of prepolymers,

$$R_g \equiv \left\{ \frac{1}{N_p N_b} \sum_{i}^{N_p} \sum_{j}^{4N_b} (\mathbf{l}_{ij} - \mathbf{l}_i^g)^2 \right\}^{1/2} \quad (6)$$

Here, $\mathbf{l}_{ij}$ is the positional vector of the jth blob within the ith prepolymer, and $\mathbf{l}_i^g$ is the position vector of the center of mass of the ith prepolymer. The results are shown in Figure 3. R_g starts to decrease at $\phi_0 \approx 0.04$, indicating that prepolymers at this concentration have started to interact with each other. The relationships $R_g \sim \phi_0^{-0.12}$ and $R_g \sim \phi_0^{-0.11}$ are observed for TB star polymers and for the combination of cross-linkers and linear polymers, respectively. This is in extremely good agreement with the scaling for a semidilute system in good solvent, $R_g \sim \phi_0^{-1/8}$.[48] From this, we determined that $\phi^* = 0.04$ for our system, which defines the normalized concentration $\Phi \equiv \phi_0/\phi^*$. Therefore, $\Phi \ll 1.0$ represents a dilute system, $\Phi \approx 1.0$ a semidilute system, and $\Phi \gg 1.0$ a concentrated system.

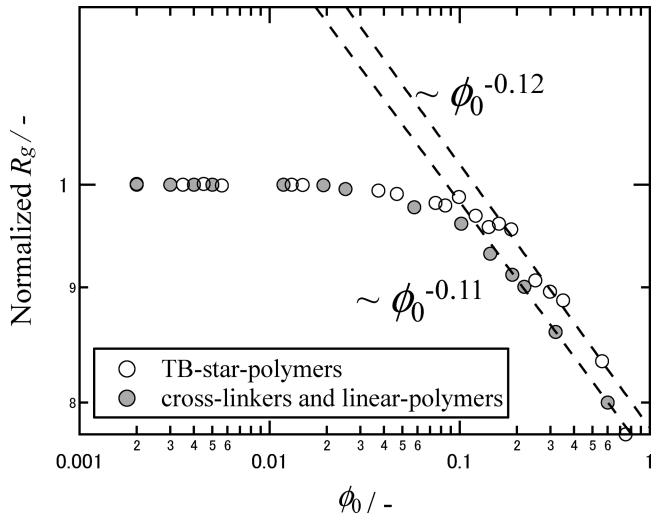

Figure 3. ϕ_0 dependence of normalized R_g of prepolymers at solution state. The dashed lines represent the scaling of normalized $R_g \sim \phi_0^{-0.12}$ and normalized $R_g \sim \phi_0^{-0.11}$ for TB star polymers and the combination of cross-linkers and linear polymers, respectively.

Links. First we discuss links in EC and CC gels. A "link" is the set of all direct connections between neighboring prepolymers. The bonding patterns of EC and CC gels are as shown in Figure 4. It is ideal that two cross-links are linked by one polymer chain, which is the "single link" in Figure 4. Generally, it is thought that the elastic modulus is proportional to the concentration of elastically effective chains (CEE). Regardless of the link type, the elastic energy stored in polymer chains between cross-links is the same.[49] Thus, the two polymer chains making up a double link count as only one elastically effective chain. In other words, in all links besides a single link, cross-links are inefficiently bonded and therefore CEE is decreased. Furthermore, a quadruple link forms an individual cluster and becomes a sol component instead of a gel, so it does not contribute to elasticity. Likewise, a self-biting link does not bond with any cross-link and also does not contribute to elasticity. Note that self-biting links can be formed in EC gels but not in CC gels. Naturally, in term of elasticity, all links besides single links are regarded as "defects" since each represent some form of elastic inefficiency.

dx.doi.org/10.1021/ma400486h | Macromolecules XXXX, XXX, XXX−XXX

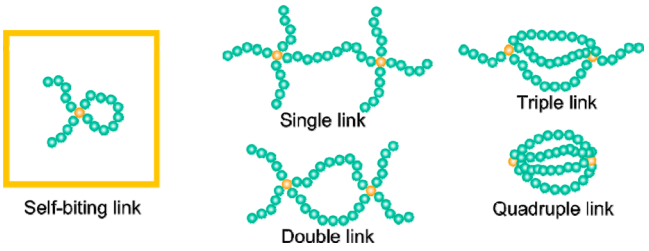

Figure 4. Schematic of formable links for CC and EC gels. Yellow blobs represent cross-links.

However, in this study, our main objective is to determine the local inhomogeneities that can affect spatial inhomogeneity. Thus, we investigate which kinds of links strongly restrict how the cluster grows and define "defects" from this perspective. For example, a triple link can restrict the cluster to grow in only one direction, whereas a single link allows the cluster to grow in six directions. These restrictions in growth direction lead to spatial inhomogeneities. Hence, we regard all links besides single links and double links as "defects". A gel with many defects is a gel with large connectivity inhomogeneity.

We report the frequency of each link type as a link fraction, that is, the number of terminal blobs participating in links of the specified type divided by the total number of terminal blobs. Each link fraction is as follows: single link, m_s; double link, m_d; triple link, m_{tri}; quadruple link, m_{quad}; and self-biting link, m_{self} (only for EC gel). m_{defect} is summation of defects. Figure 5 shows the Φ dependence of each link fraction of EC and CC gels at the final state. For CC gels, we found that single links had largest population, followed by double links, with all others having much smaller populations. Note that single links monotonically increased while all other links monotonically decreased with increasing Φ. In other words, connectivity inhomogeneities monotonically decreased with increasing Φ. These results are in pretty good agreement with those of Lange et al.[43,44] Also note that in both CC and EC gels the fraction of single links is almost the same. The conventional definition of defects (all links besides single links) would suggest that both gels have about the same amount of "defects". However, there is a difference in the types of the most prevalent of defects between the two gels. In EC gels, most of the defects are self-biting links, but in CC gels most are double links. This tendency agrees well with assertion by Schwenke et al.[43] that EC gels have many elastically inactive bonds that do not exist in CC gels, and these are probably the cause of the significant degradation in elasticity of EC gels. From this, we assert that it is not favorable to perceive gels with conventional concept of defects. Hence, we compare EC and CC gels with our definition of defects and show these results in Figure 6. From this definition, EC gels have more defects than CC gels at any given concentration, which indicates that EC gels have larger connectivity inhomogeneities than CC gels. The essential difference between the two gels could be regarded as whether or not a gel contains self-biting links.

Cycles. Here, we discuss the concept of cycles. While a "link" is based only on the bonding of neighboring prepolymers, a "cycle" is defined as the polygonal shape formed by several prepolymers. The algorithm to identify cycles is as follows. First, we consider a cross-point. For convenience, let us call this as cross-point 1. Here, cross-point is the cross-linker in EC gels and the joining bead of four polymer chains of prepolymer in CC gels. Next, we search neighbor cross-point 2 that connects to cross-point 1 via only one network strand. Then, we find cross-point 3,

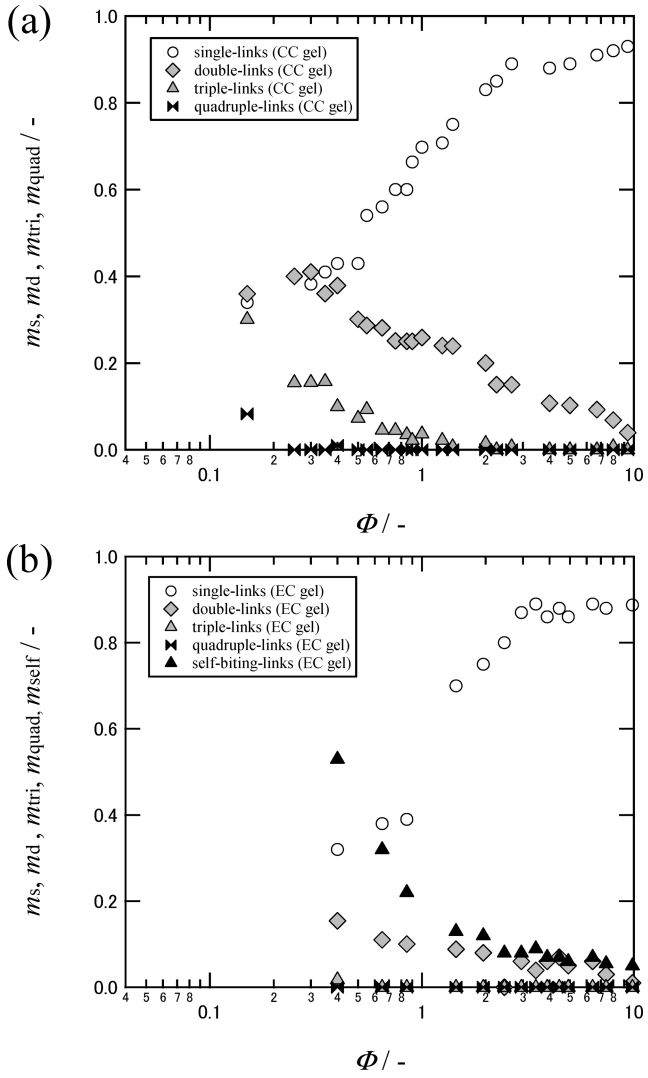

Figure 5. Φ dependence of m_s, m_d, m_{tri}, m_{quad}, and m_{self} at the final state: (a) CC gels; (b) EC gels.

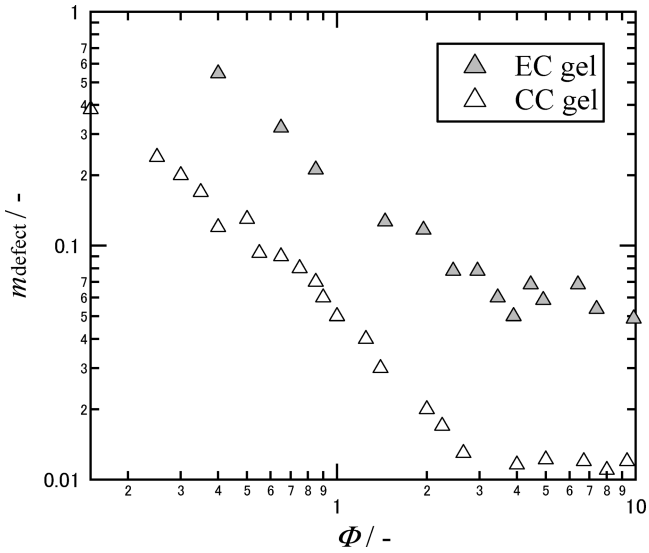

Figure 6. Comparison of m_{defect} between CC and EC gels.

which connects to cross-point 2 via only one network strand. We also confirm that cross-point 3 does not connect with cross-point

dx.doi.org/10.1021/ma400486h | Macromolecules XXXX, XXX, XXX−XXX

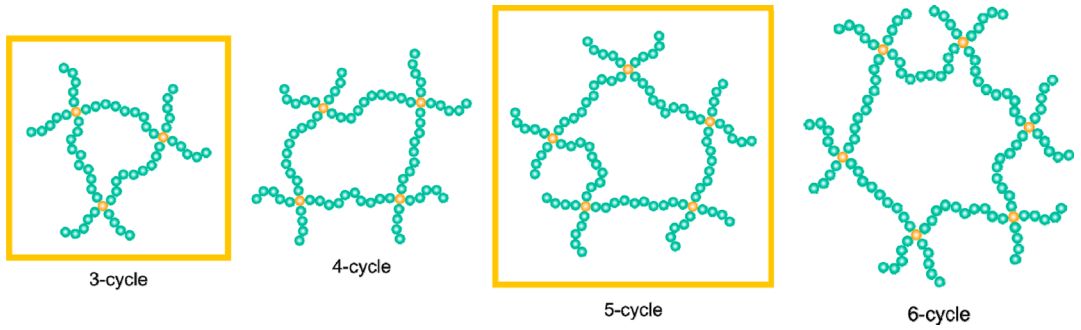

Figure 7. Schematic of formable cycles of CC and EC gels. Yellow blobs represent cross-links. Note that triple- and penta-cycles are formable only in EC gels.

1 in any way. We repeat the same process for other cross-points. As the size of a cycle becomes larger, there is a high probability that a cross-point i connects to a cross-point j via several network strands. In other words, there may be a smaller cycle contained within a larger cycle via sharing several cross-points. The cycle structure becomes too complex, and it is meaningless to quantify such cycles. We found that the number of octa-cycles in a CC gel estimated by our method was larger than the number of hexa-cycles by 2 orders of magnitude. This indicates that there are many octa-cycles that are not "independent". Because it is difficult to identify independent octa-cycles, we focus only on smaller cycles.

Formable cycles of EC and CC gels are shown in Figure 7. Note that in CC gels only quadruple cycles and hexa-cycles are formable, but in EC gels all cycles are formable. Because of this difference alone, it is very likely that EC gels have more variation of cycles than CC gel, which may lead to large connectivity inhomogeneities in term of links.

In this section, we explain how cycles are quantified. Cross-links serve as vertices in cycles, and each cross-link may serve as a vertex for more than one cycle. For each type of cycle, we averaged the number of cycles of this type that each cross-link serves as a vertex for. The average for each cycle is expressed as follows: triple cycle: n_{tri}, quadruple cycle: n_{quad}, pentacycle: n_{penta}, hexacycle: n_{hexa}. Collectively, this is expressed as n_α (α = triple, quadruple, penta, hexa). For example, if cross-link A serves as a vertex for two hexa-cycles and cross-link B serves as a vertex for four hexa-cycles, then n_{hexa} is 3.0. Figure 8 shows the Φ dependence of n_α at the final state. For CC gels, hexa-cycles are most prevalent. With increasing Φ, n_{hexa} increases and n_{quad} decreases. For EC gels, hexa-cycles are also most prevalent. With increasing Φ, n_{hexa} increases but n_{penta}, n_{quad}, and n_{tri} hardly change. The cycles besides hexa-cycles exist in almost the same amounts, and there are several more types of these cycles ithin EC gels compared to CC gels, which indicates that EC gels have larger connectivity inhomogeneities than CC gels in term of cycles.

Correlation between Links and Spatial Inhomogeneities. As discussed above, we have quantified links and cycles and have clarified that EC gels have larger connectivity inhomogeneity (larger variation of cycles) than CC gels. Next, we discuss the correlation between defects and spatial inhomogeneities. First, we quantify spatial inhomogeneities. We calculated the radial distribution function $g(r)$ of gels at the final state (p = 0.95), which is calculated from the position coordinates of all blobs that make up the infinite network, as

$$g(r) = \frac{1}{4\pi r^2 \rho \Delta r} \langle \sum_{i}^{N_{max}} n_i(r) \rangle \tag{8}$$

where N_{max} is the number of blobs included in the infinite network, ρ is density, and $n_i(r)$ is the number of blobs between

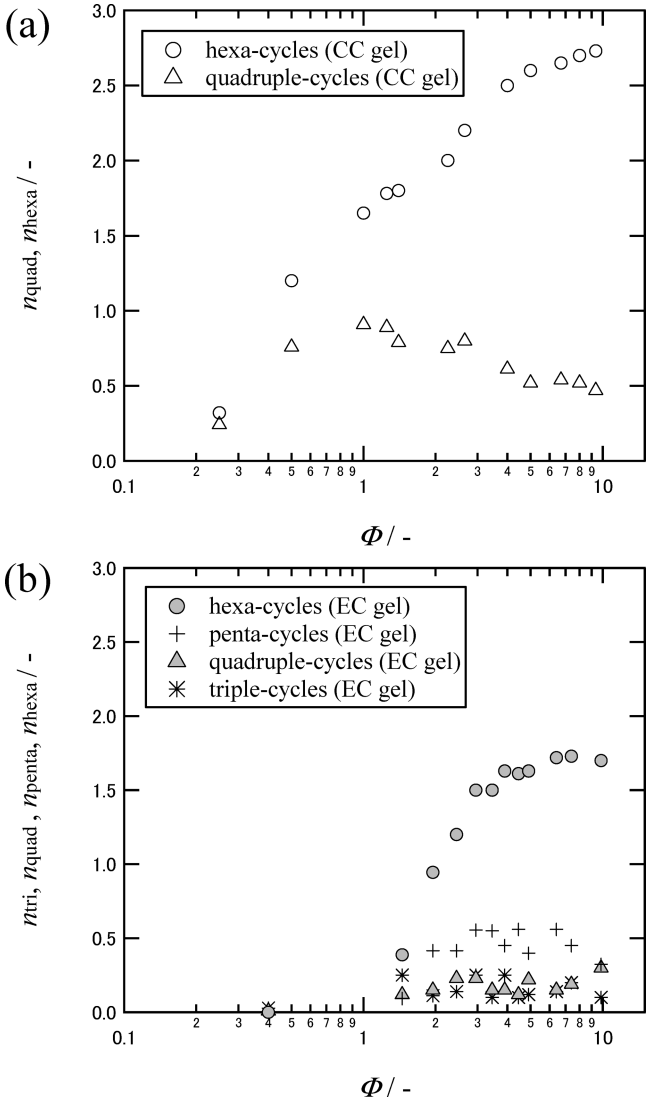

Figure 8. Φ dependence of n_α at the final state: (a) CC gels; (b) EC gels.

r and $r + \Delta r$. We chose Δr = 0.005. The correlation length ξ is fitted from $g(r)$ for each sample using the following function:

$$g(r) \propto \frac{1}{r} \exp\left(-\frac{r}{\xi}\right) + 1 \tag{9}$$

Equation 9 is the correlation for a blob system with size ξ. Examples of obtained $g(r)$ are shown in Figure 9. Results fitted by eq 9 are shown as dashed lines, and eq 9 fits well to all $g(r)$

dx.doi.org/10.1021/ma400486h | Macromolecules XXXX, XXX, XXX−XXX

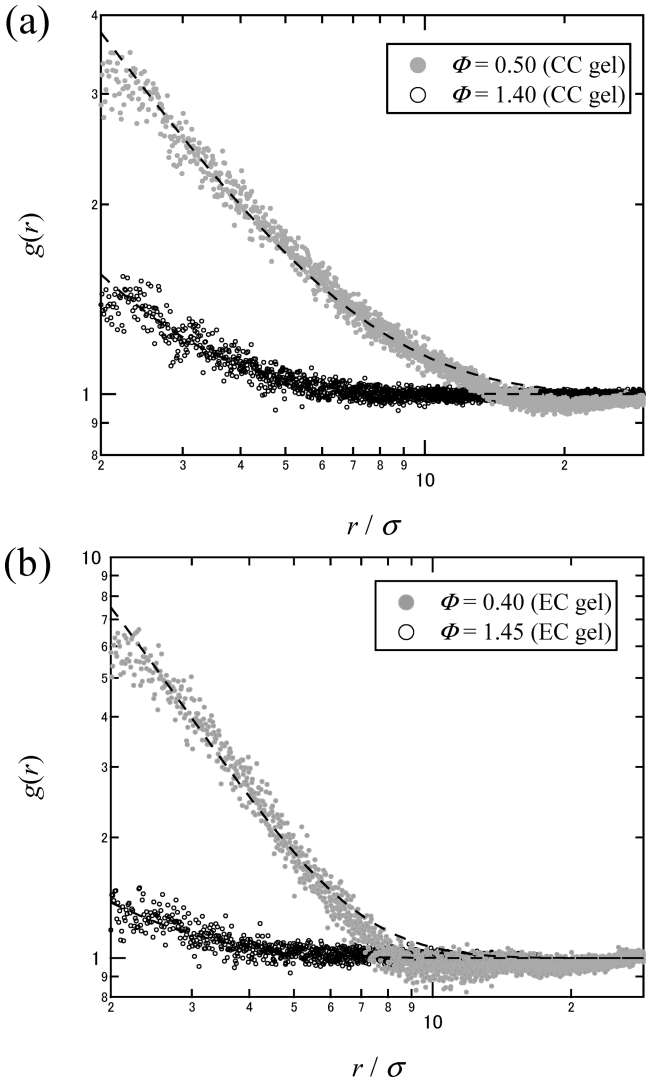

Figure 9. Comparison of $g(r)$ at the final state: (a) CC gel; (b) EC gel. Dashed lines represent results of fitting by eq 9.

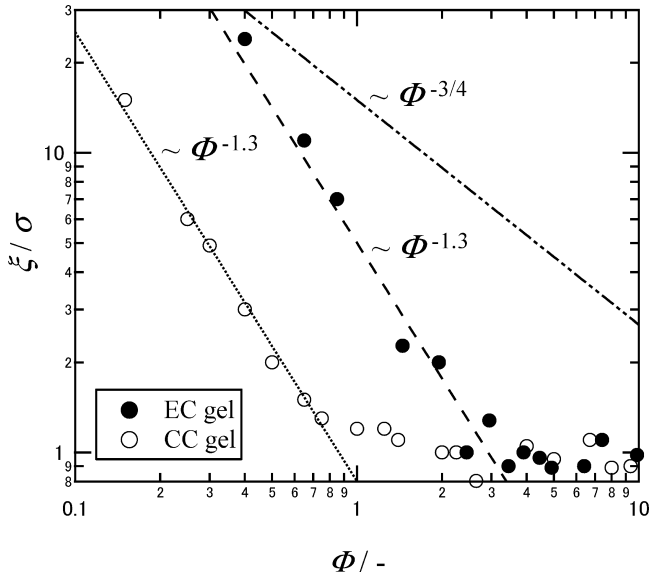

Figure 10. Φ dependence of ξ at the final state for CC and EC gels. Dots and dashed lines represent $\xi \sim \Phi^{-1.3}$. The broken line represents $\xi \sim \Phi^{-3/4}$.

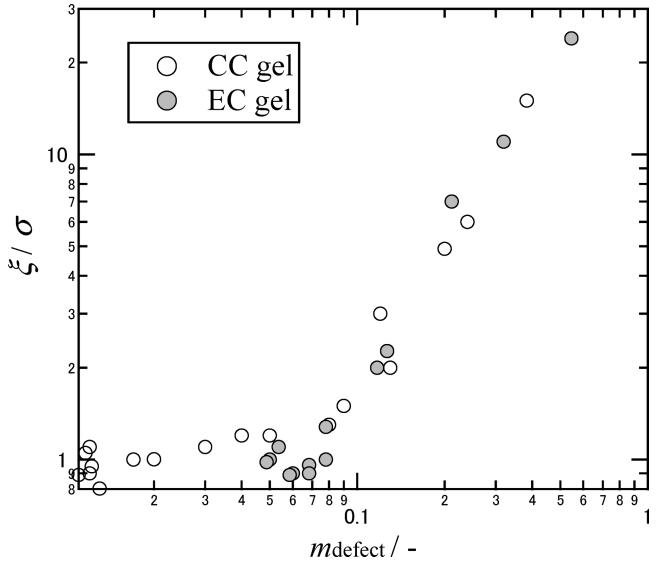

Figure 11. Relationship between ξ and m_{defect} at the final state for CC and EC gels.

observed. In a dilute system, $g(r)$ rises sharply at short distance, and a long tail is observed for EC and CC gels. This indicates that there is a long distance correlation in a dilute system. On the other hand, a long tail was not observed in a concentrated system. This indicates that long distance correlation was lost. Figure 10 shows the Φ dependence of ξ for EC and CC gels. For concentrated systems, ξ is almost constant ($\approx 1.0\sigma$). This is an artifact of our model owing to the fact that ξ cannot be smaller than the blob size. Hence, we could not observe the correct ξ scaling for concentrated systems due to this limitation. For dilute and semidilute systems, ξ increases with decreasing Φ as $\xi \sim \Phi^{-1.3}$. This tendency roughly agrees with neutron scattering results of Tetra-PEG gels.[19] On the other hand, de Gennes et al. have predicted as $\xi \sim \Phi^{-3/4}$.[48] According to Matsunaga et al., this disagreement has been interpreted as follows. In a dilute system, a large number of defects might form, thus preventing the gel to grow into an ideal network, and this results in a larger mesh size.[19] However, this assumption has not yet been verified. Therefore, we investigated the correlation between the obtained ξ and fractions of defects m_{defect}. Figure 11 shows the relationship between ξ and m_{defect}. The trend changes abruptly at $m_{defect} \approx 0.15$. For $m_{defect} < 0.15$, corresponding to concentrated system, the true correlation between ξ and m_{defect} could not be observed for the reason described above. For $m_{defect} > 0.15$, which roughly corresponds to the semidilute regime, ξ monotonically increases with increasing m_{defect}. This indicates a strong correlation between the fraction of defects and the spatial inhomogeneities in dilute and semidilute systems.

In this passage, we closely examine the spatial inhomogeneity in concentrated systems. As indicated in Figure 10, we did not observe large spatial inhomogeneity in both EC and CC gels. As discussed in previous studies, inhomogeneities are more apparent in swollen gels than in as-prepared gels.[16,50] Therefore, we remeasured the spatial inhomogeneities in artificially swollen gels. We adopted the following method to artificially swell the gels. In one MD step, the coordinates of cross-links and the dimensions of the periodic cell are increased by a factor of 1.001 in the x, y, and z directions. Following this, the system is stabilized with 10^5 MD steps. This process is repeated. Since the

dx.doi.org/10.1021/ma400486h | Macromolecules XXXX, XXX, XXX−XXX

relaxation time of such a complex topological structure is much longer than the stabilization period, the artificially swollen structures are not fully comparable with real swollen networks. However, the purpose of this artificial swelling process is only to let hidden spatial inhomogeneities emerge. The final gel concentration Φ_m is 0.15 for the CC gel (Φ = 5.00) and 0.15 for the EC gel (Φ = 4.90). $g(r)$ of the swelled gels is shown in Figure 12. First, in the short distance region, $g(r)$ rises sharply,

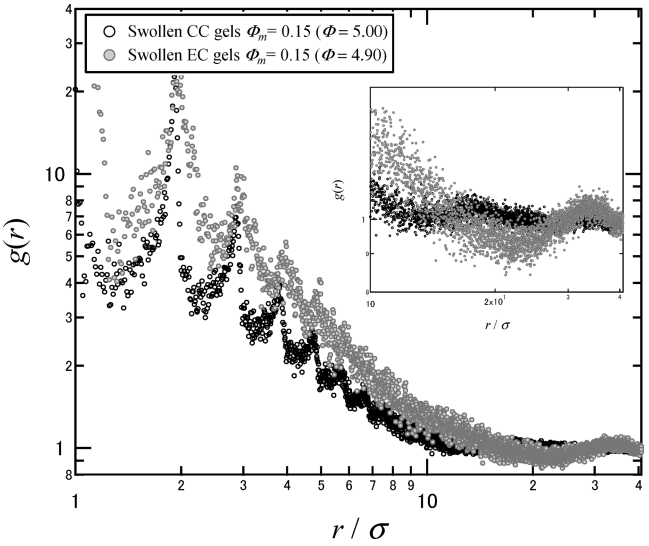

Figure 12. Comparison of $g(r)$ between swollen CC and EC gel. The inset shows magnification of the long distance region. CC gel: Φ_m = 0.15 (Φ = 5.00). EC gels: Φ_m = 0.15 (Φ = 4.90).

and peaks at equal intervals (interval ≈ 1.10) are observed. This interval is close to fully stretched distance R_0 = 1.5 between blobs in the KG model. These peaks are ascribed to correlation of blobs within a stretched cross-link chain. In other words, it is found that the artificially swollen gels are very similar to a fully stretched state. Note that these peaks of correlation of blobs cannot be observed in experiments because they are only an artifact of the simulation model. The blobs have a defined size, but in reality, they represent a hypothetical region of Gaussian chains. On the other hand, there is a significant difference between the EC and CC gels at long distance. In the CC gel, $g(r)$ decays at a shorter distance than the EC gel and converges to the average density of system ($g(r)$ = 1.0). However, in the EC gel, $g(r)$ has a longer tail than in the CC gel and displays a pronounced minimum at r = 20σ. This range is about 10% more dilute than the average density of system. Moreover, a large correlation peak is observed at r = 30σ. It is interpreted that such peaks of $g(r)$ at long distance are cluster−cluster interferences. Therefore, we interpret this peak in our system as follows. When the EC gel is swollen, the network can be pictured as a network of island structures (regions with an approximate size of 20σ) connected by stringlike structures. In other words, spaces of lower density between islands in the swollen EC gel are large spatial inhomogeneities.

In this section, we investigate the correlation between this spatial heterogeneity and self-biting links. Cross-linkers that form self-biting links do not contribute to forming three-dimensional networks and thus cannot be cross-links. Therefore, it is expected that after swelling the structure around self-biting links has low density. To verify this assumption, we investigated variation of $g(r)_{self}$ around cross-links during the swelling process and compared it with $g(r)$ of the whole system (see Figure 13). Note

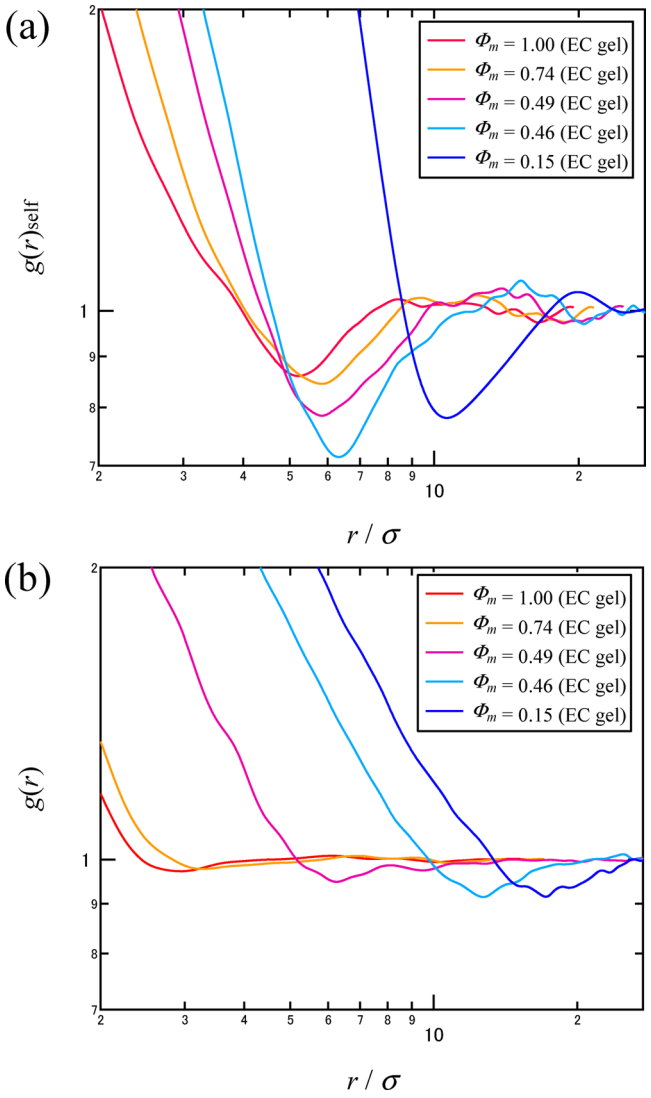

Figure 13. Comparison of $g(r)_{self}$ and $g(r)$ of the EC gel during the swelling process.

that a low-pass filter was used for $g(r)$ so that the data are easier to understand. As the system swelled, structure around self-biting links became markedly low in density, compared with the density of whole system. These results indicate that the large spatial inhomogeneities observed in swollen gels co-occur with the density drop in the network around self-biting links.

Behavior of Cycles during Swelling Process. In above sections, we have investigated artificially swollen concentrated systems and observed the spatial inhomogeneities that are generated around the self-biting links, which cannot form three-dimensional networks. In this section, we discuss the behavior of cycles during the swelling process. As mentioned before, several types of cycles coexist within CC gels and EC gels, especially in concentrated systems. We expect that the way each cycle swells strongly correlates to the way that spatial inhomogeneities are ultimately formed within the system.

Let us define the linear swelling ratio λ. Figure 14 shows the relationship between R_g* and λ. Here, R_g* is the average radius of gyration of each cycle normalized by its radius of gyration before the swelling. It is equal to the linear swelling ratio in a cycle. The samples used in Figure 12 correspond to the case of λ = 3.2. As shown in Figure 14a, in CC gels, the degree of swelling of

dx.doi.org/10.1021/ma400486h | Macromolecules XXXX, XXX, XXX−XXX

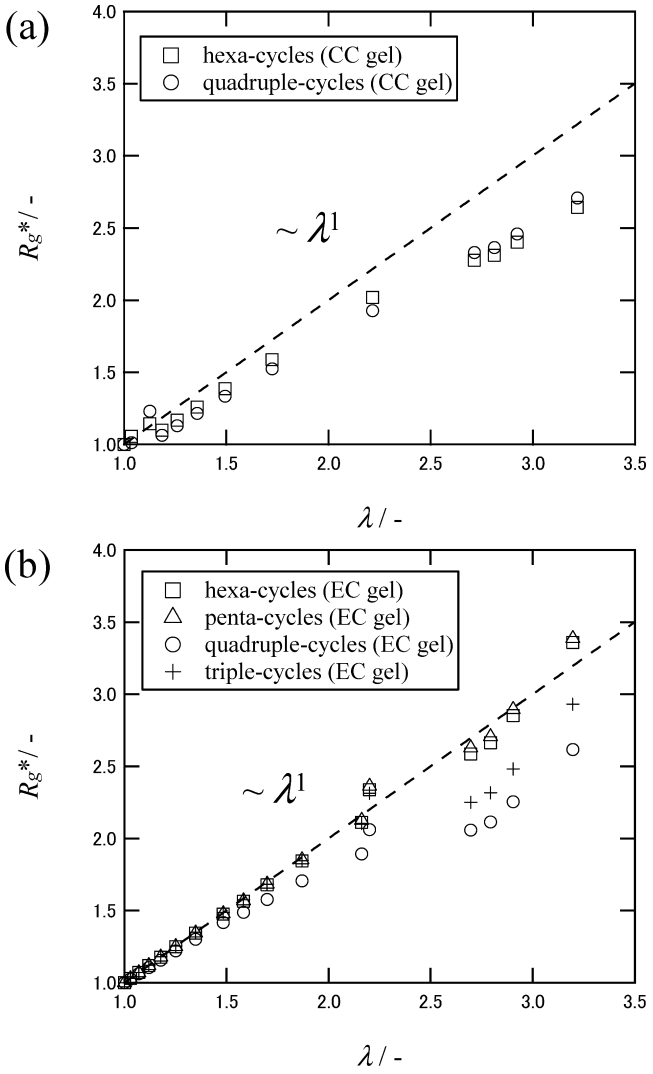

Figure 14. Comparison of R_g^* between swollen CC and EC gels. Dashed lines represent $R_g^* \sim \lambda^1$. (a) CC gels: $\Phi_m = 0.15$ ($\Phi = 5.00$). (b) EC gels: $\Phi_m = 0.15$ ($\Phi = 4.90$).

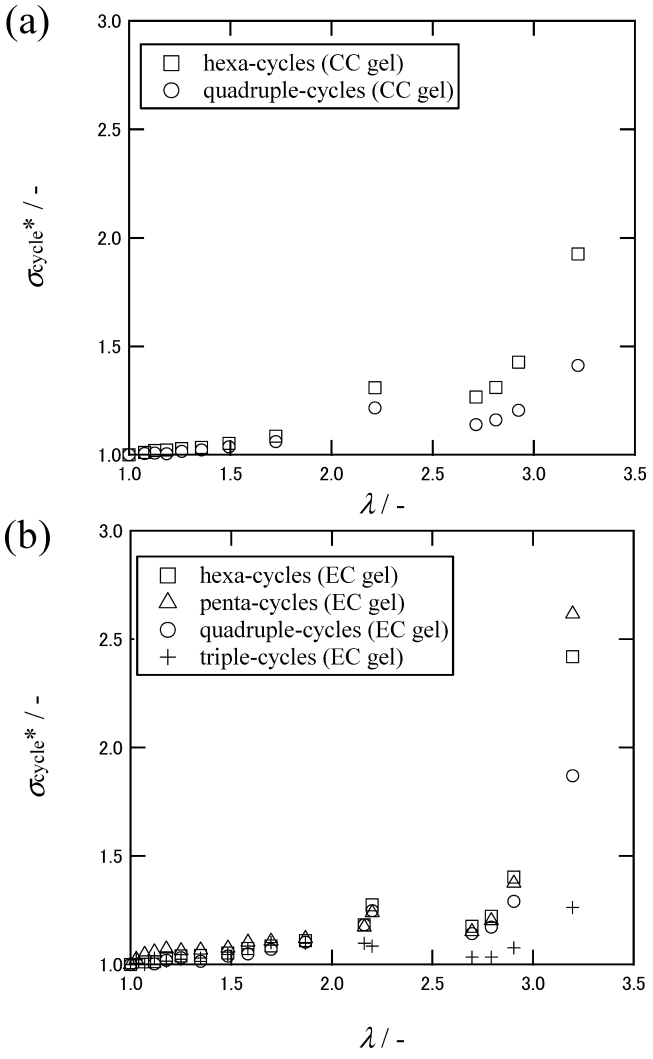

Figure 15. Comparison of σ_{cycle}^* between swollen CC and EC gels. CC gels: $\Phi_m = 0.15$ ($\Phi = 5.00$). EC gels: $\Phi_m = 0.15$ ($\Phi = 4.90$).

quadruple- and hexa-cycles could be expressed as $R_g^* \sim \lambda^1$ for low λ. This indicates that at low λ quadruple- and hexa-cycles are swollen as large as the gel as a whole. At large λ, the degrees of swelling of quadruple- and hexa-cycles are smaller than that of the gel in whole. Note that the degrees of swelling of quadruple- and hexa-cycles are almost same. In other words, quadruple- and hexa-cycles are transformed collectively. On the other hand, for EC gels, the degree of swelling of penta- and hexa-cycles could be expressed as $R_g^* \sim \lambda^1$ (see Figure 14b). However, triple- and quadruple-cycles exhibit a plateau in swelling from $\lambda \approx 2.0$ to $\lambda \approx 2.8$, after which they start to swell again. This could be interpreted as follows. Until $\lambda \approx 2.0$, all cycles are swollen almost equally. Then, difference in swelling between cycles start to appear. Since penta- and hexa-cycles have large ring structures, they are more flexible than triple- and quadruple-cycles and can swell greatly. However, triple- and quadruple-cycles have smaller ring structures and cannot swell as much. Therefore, penta- and hexa-cycles can continue to swell, while triple- and quadruple-cycles cannot. This corresponds to the region from $\lambda \approx 2.0$ to $\lambda \approx 2.8$. Triple- and quadruple-cycles are swollen obligatorily after $\lambda \approx 2.8$.

Furthermore, we investigated λ dependence of average force (stress) per one bead in each cycle. Figure 15 shows the relationship between σ_{cycle}^* and λ. Here, σ_{cycle}^* is the average force per one bead of each cycle normalized by the average force per one bead before swelling. The average force is calculated as average of the force upon blobs which compose the cycle. As shown in Figure 15a, for CC gels, the σ_{cycle}^* of each type of cycle increases with increasing λ. Each cycle exhibits similar behavior until $\lambda \approx 2.5$. At a larger λ, the σ_{cycle}^* of hexa-cycles becomes larger than that of quadruple-cycles. The σ_{cycle}^* of hexa-cycles is a maximum of about 1.3 times larger than that of quadruple-cycles. For EC gels, the σ_{cycle}^* of each cycle increases with increasing λ. Each cycle exhibits a similar behavior until $\lambda \approx 2.5$. At higher λ, differences between cycles start to appear. A maximum of about 2.5 times disparity is observed between the largest and smallest σ_{cycle}^*. This disparity is much higher than that of CC gels. In other words, since EC gels have more variation in cycles compared to CC gels, the difference in σ_{cycle}^* between different types of cycles is much higher.

Furthermore, we analyzed the stress distribution of each cycle (shown in Figure 16). In this figure, both EC and CC gels in the as-prepared state do not show any difference in the stress distribution of beads that form each cycle. We found that the distribution could be fitted by a Gaussian distribution for all cycles. On the other hand, in swollen gels, the variance of stress distribution is larger. This implies that stress is generated with the

dx.doi.org/10.1021/ma400486h | Macromolecules XXXX, XXX, XXX−XXX

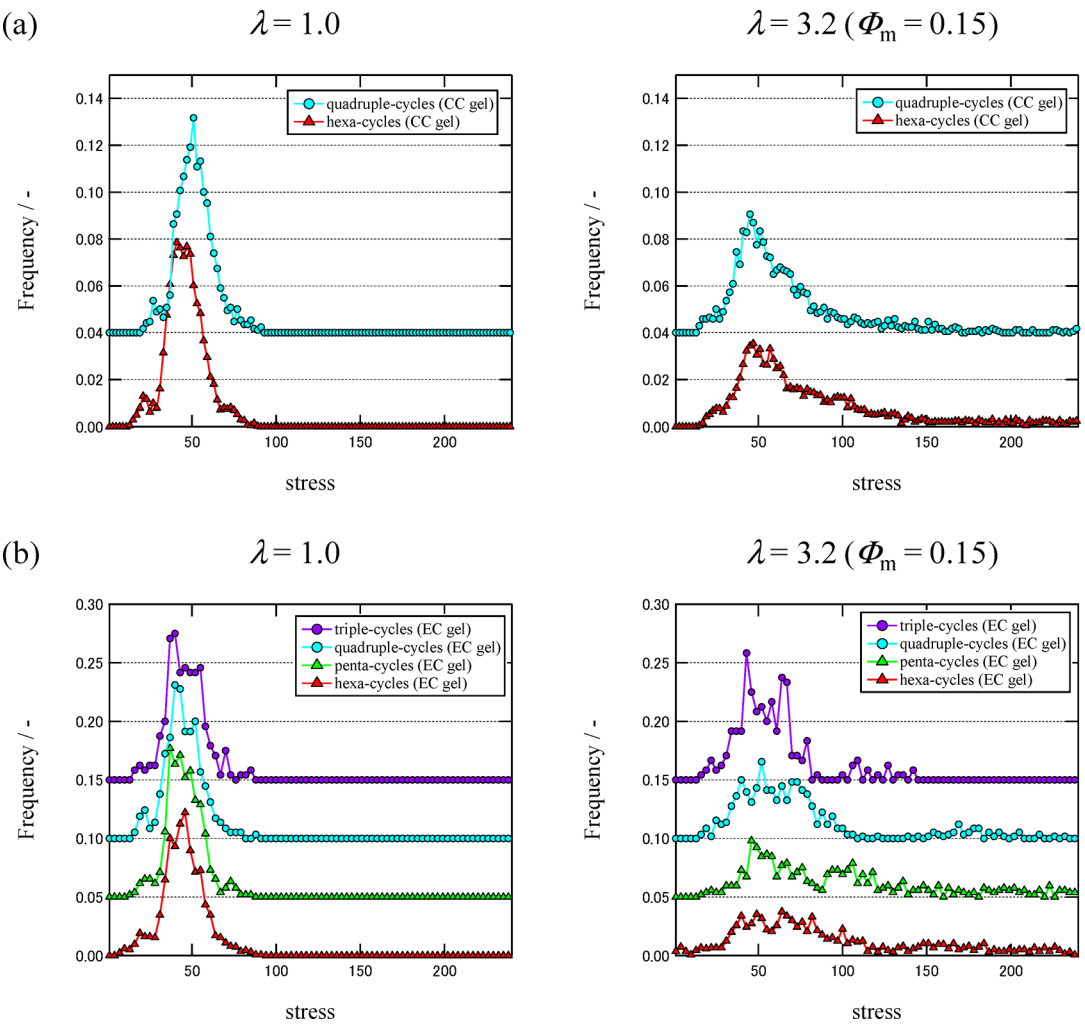

Figure 16. Change of stress distribution between as-prepared and swollen gels. Left figures: as-prepared gels. Right figures: swollen gels. (a) CC gels: Φ = 5.00. (b) EC gels: Φ = 4.90.

swelling of gel. In CC gels, hardly any difference between cycles is observed; all beads feel the same stress under similar conditions. It could be said that CC gels have a uniform stress distribution. However, in EC gels, there is a significant difference between cycles in their stress distribution. For each cycle, the stress distribution is extremely broad; hexa-cycles have the broadest variance, then penta-cycles, then quad-cycles, and last tricycles have the least broad distribution. Moreover, the stress distribution of hexa- and penta-cycles has a tail in the range of extremely high stress, implying that stress concentrates on larger cycles as the swelling progresses. Furthermore, since the stress in this range is 3−4 times the average stress, these cycles are likely close to their fully stretched state. Thus, when the gel is further swollen, the network strands of these large cycles are more prone to breakage.

From discussions above, the physical picture during swelling process could be described as follows. First, at a small degree of swelling, all cycles swell uniformly. As the swelling degree becomes larger, the network around self-biting links can no longer swell uniformly. Low density space starts to appear around these links, and the space broadens. As swelling progresses further, the difference in the swelling degree of different types of cycles becomes more evident, and the stress on each cycle becomes inhomogeneous. These differences become more significant when the gel contains a greater variety of cycles. Because of this, spatial inhomogeneities that are not observed in gels in their as-prepared state appear in swollen gels. To put it plainly, a way to possibly reduce spatial spatial inhomogeneities in the swollen state is to create gels that do not contain self-biting links or cycle variations, such as A−B network gels like the Tetra-PEG gel.

■ CONCLUSIONS

We simulated the gelation process using molecular dynamics and investigated the correlation between spatial and connectivity inhomogeneities of gels. We compared EC and CC gels, and as a result, the following five points were revealed. (1) EC gels have more "defects" than CC gels. Here, "defects" are links such as self-biting links that strongly restrict connection with three-dimensional network. (2) Such defects lead to low density structures within the gels, which lead to large spatial inhomogeneities. (3) During the swelling process, the low density space spreads around "defects", especially self-biting links. (4) When EC gels are swollen, each cycle has a different degree of swelling, leading to large spatial inhomogeneities. (5) As swelling progresses, the stress on each cycle becomes inhomogeneous and concentrates more on larger cycles.

From the above discussion, we were able to indicate that spatial inhomogeneities in gels are caused by connectivity inhomogeneities. Furthermore, the degree of connectivity

dx.doi.org/10.1021/ma400486h | Macromolecules XXXX, XXX, XXX−XXX

inhomogeneity depends strongly on the structures of the prepolymers. To realize the model network, it is necessary to design prepolymers that allow a smaller set of formable defects (especially to exclude self-biting links and to limit the variety of cycles), which is the case for CC gels.

AUTHOR INFORMATION

Corresponding Author

*E-mail ma3284@columbia.edu (M.A.).

Present Address

[§]M.A.: Department of Chemical Engineering, Columbia University, 801 Mudd; 500 W 120th St., New York, NY 10027.

Notes

The authors declare no competing financial interest.

ACKNOWLEDGMENTS

We thank Dr. Sinkovits and Ms. Kojima for preparing this manuscript. This research is supported by the Ministry of Education, Science, Sports and Culture, Japan Grant-in-Aid for Scientific Research, Grant No. 2224518 to M.S. We thank the Supercomputer Center, Institute for Solid State Physics, University of Tokyo, for the use of facilities and the SGI Altix ICE 8400EX (and/or NEC SX-9).

REFERENCES

(1) Drury, J. L.; Mooney, D. J. *Biomaterials* **2003**, *24*, 4337−4351.
(2) Azab, A. K.; Orkin, B.; Doviner, V.; Nissan, A.; Klein, M.; Srebnik, M.; Rubinstein, A. *J. Controlled Release* **2006**, *11*, 281−289.
(3) Peppas, N. A.; Hilt, J. Z.; Khademhosseini, A.; Langer, R. *Adv. Mater.* **2006**, *18*, 1345−1360.
(4) Bryant, S. J.; Bender, R. J.; Durand, K. L.; Anseth, K. S. *Biotechnol. Bioeng.* **2004**, *86*, 747−755.
(5) Stein, R. S. *J. Polym. Sci.* **1969**, *B7*, 657−660.
(6) Pines, E.; Prins, W. *J. Polym. Sci., Polym. Phys. Ed.* **1972**, *B10*, 719−724.
(7) Candau, S.; Bastide, J.; Delsanti, M. *Adv. Polym. Sci.* **1982**, *44*, 27.
(8) Panyukov, S.; Rabin, Y. *Macromolecules* **1996**, *29*, 7960−7975.
(9) Bastide, J.; Candau, S. J. Structure of Gels as Investigated by Means of Static Scattering Techniques. In *The Physical Properties of Polymer Gels*; Cohen Addad, J. P., Ed.; John Wiley: New York, 1996; Chapter 9, p 143.
(10) Shibayama, M. *Macromol. Chem. Phys.* **1998**, *199*, 1−30.
(11) Shibayama, M.; Norisuye, T. *Bull. Chem. Soc. Jpn.* **2002**, *75*, 641−659.
(12) Mallam, S.; Horkay, F.; Hecht, A. M.; Geissler, E. *Macromolecules* **1989**, *22*, 3356.
(13) Mendes, E. J.; Lindner, P.; Buzier, M.; Boue, F.; Bastide, J. *Phys. Rev. Lett.* **1991**, *66*, 1595.
(14) Mendes, E.; Girard, B.; Picot, C.; Buzier, M.; Boue, F.; Bastide, J. *Macromolecules* **1993**, *26*, 6873−6877.
(15) Bastide, J.; Leibler, L. *Macromolecules* **1988**, *21*, 2647.
(16) Shibayama, M.; Shirotani, Y.; Shiwa, Y. *J. Chem. Phys.* **2000**, *112*, 442−449.
(17) Pusey, P. N.; van Megen, W. *Physica A* **1989**, *157*, 705−741.
(18) Joosten, J. G. H.; Gelade, E. T. F.; Pusey, P. N. *Phys. Rev. A* **1990**, *42*, 2161−2175.
(19) Matsunaga, T.; Sakai, T.; Akagi, Y.; Chung, U. I.; Shibayama, M. *Macromolecules* **2009**, *42* (16), 6245−6252.
(20) Dusek, K. *Trends Polym. Sci.* **1997**, *5*, 268−274.
(21) Hild, G. *Prog. Polym. Sci.* **1998**, *23*, 1019−1149.
(22) Malkoch, M.; Vestberg, R.; Gupta, N.; Mespouille, L.; Dubois, P.; Mason, A. F.; Hedrick, J. L.; Liao, Q.; Frank, C. W.; Kingsbury, K.; Hawker, C. *J. Chem. Soc., Chem. Commun.* **2006**, *26*, 2774−2776.
(23) Durackova, A.; Valentova, H.; Duskova-Smrckova, M.; Dusek, K. *Polym. Bull.* **2007**, *58*, 201−211.
(24) Shibayama, M.; Takahashi, H.; Nomura, S. *Macromolecules* **1995**, *28*, 6860−6864.
(25) Villar, M. A.; Valles, E. M. *Macromolecules* **1996**, *29*, 4081−4089.
(26) Patel, S. K.; Malone, S.; Cohen, C.; Gillmer, J. R.; Colby, R. H. *Macromolecules* **1992**, *25*, 5241−5251.
(27) Sakai, T.; Matsunaga, T.; Yamamoto, Y.; Ito, C.; Yoshida, R.; Suzuki, S.; Sasaki, N.; Shibayama, M.; Chung, U. I. *Macromolecules* **2008**, *41* (14), 5379−5384.
(28) Matsunaga, T.; Sakai, T.; Akagi, Y.; Chung, U.; Shibayama, M. *Macromolecules* **2009**, *42* (4), 1344−1351.
(29) Tonelli, A. E.; Helfand, E. *Macromolecules* **1974**, *7*, 59−63.
(30) Helfand, E.; Tonelli, A. E. *Macromolecules* **1974**, *7*, 832−834.
(31) Dusek, K.; Gordon, K.; Ross-Murphy, S. B. *Macromolecules* **1978**, *11*, 236−245.
(32) Dusek, K. In *Developements in Polymerisation-3*; Applied Science Publishers: London, 1982.
(33) Llorente, M. A.; Mark, J. E. *J. Chem. Phys.* **1979**, *71*, 682−689.
(34) Gottlieb, M.; Macosko, C. W.; Benajamin, G. S.; Meyers, K. O.; Merill, E. W. *Macromolecules* **1981**, *14*, 1039−1046.
(35) Patel, S. K.; Malone, S.; Cohen, C.; Gillmor, J. R.; Colby, R. H. *Macromolecules* **1992**, 5241−5251.
(36) Trautenberg, H. L.; Sommer, J. U.; Goritz, D. *Macromol. Symp.* **1994**, *81*, 153−160.
(37) Lee, K. J.; Eichinger, B. E. *Macromolecules* **1988**, *22*, 1441−1448.
(38) Leung, Y.-K.; Eichinger, B. E. *J. Chem. Phys.* **1984**, *80* (8), 3885−3892.
(39) Leung, Y.-K.; Eichinger, B. E. *J. Chem. Phys.* **1984**, *80*, 3877−3884.
(40) Grest, G. S.; Kremer, K. *Macromolecules* **1990**, *23*, 4994−5000.
(41) Shy, L. Y.; Eichinger, B. E. *Macromolecules* **1986**, *19*, 2787−2793.
(42) Lang, M.; Goritz, D.; Kreitmeier, S. *Macromolecules* **2003**, *36*, 4646−4658.
(43) Schwenke, K.; Lang, M.; Sommer, J.-U. *Macromolecules* **2011**, *44* (23), 9464−9472.
(44) Lange, F.; Schwenke, K.; Kurakazu, M.; Akagi, Y.; Chung, U.; Lang, M.; Sommer, J.-U.; Sakai, T.; Saalwaechter, K. *Macromolecules* **2011**, *44*, 9666−9674.
(45) Langer, M.; Goritz, D.; Kreitmeier, S. *Macromolecules* **2005**, *38*, 2515−2523.
(46) Carmesin, I.; Kremer, K. *Macromolecules* **1988**, *21* (9), 2819−2823.
(47) Kremer, K.; Grest, G. S. *J. Chem. Phys.* **1990**, *92* (8), 5057−5087.
(48) de Gennes, P. G. *Scaling Concepts in Polymer Physics*; Cornell University Press: Ithaca, NY, 1979.
(49) Akagi, Y.; Matsunaga, T.; Shibayama, M.; Chung, U.; Sakai, T. *Macromolecules* **2010**, *43* (1), 488−493.
(50) Bastide, J.; Leibler, L.; Prost, J. *Macromolecules* **1990**, *23* (6), 1821.